RESISTING METAL FATIGUE IN AEROENGINES, SURFACE DAMAGE AND SURFACE TREATMENTS

JIM BYRNE*[1], RICARDO A. CLÁUDIO[2], ANDREW BURGESS[1]

[1]Department of Mechanical and Design Engineering, University of Portsmouth, Portsmouth, UK, PO1 3DJ.
[2]Department of Mechanical Engineering, ESTSetúbal / Instituto Politécnico de Setúbal, Campus do IPS, Estefanilha, 2910-761 Setúbal.
jim.byrne@port.ac.uk

ABSTRACT: The potential failure modes of components in aero engines are considered, with particular emphasis on fatigue, including high cycle fatigue (HCF), low cycle fatigue (LCF) and combined HCF/LCF. Some results of recent studies at Portsmouth of the influence of foreign object damage (FOD) on the fatigue behaviour under these different conditions of a fan and compressor material, Ti6Al4V alloy, are presented. A two parameter crack propagation model is considered.

The benefits in resisting fatigue through surface modification by the traditional process of shot peening has become well established for components such as turbine and compressor discs. The beneficial results of shot peening on the fatigue resistance of an advance nickel base superalloy at elevated temperature are presented together with the effects of subsequent surface scratch damage.

Keywords: High Cycle Fatigue, Low Cycle Fatigue, Foreign Object Damage, Shot Peening.

RESUMO: O presente artigo refere-se ao estudo de potenciais falhas em motores de avião, em particular falhas por fadiga, incluindo fadiga a elevado de ciclos, fadiga oligocíclica e fadiga combinada. São apresentados alguns resultados, obtidos em Portsmouth, da influência de dano provocado por objectos estranhos no comportamento à fadiga das pás da fan de compressor na liga Ti6Al4V. É considerado um modelo de propagação baseado em dois parâmetros.

Em componentes como discos de turbina e compressor, a melhoria de propriedades à superfície por processos tradicionais tem trazido grandes benefícios tem termos de melhoria de resistência à fadiga. São apresentados alguns resultados do benefício da grenalhagem, na resistência à fadiga de superligas de níquel a alta temperatura, em conjunto com os efeitos de um subsequente dano à superfície causado por um pequeno risco.

Palavras chave: Fadiga a elevado número de ciclos, fadiga oligocíclica, dano por objectos estranhos, grenalhagem.

PART A - FOREIGN OBJECT DAMAGE

1. INTRODUCTION

Foreign object damage (FOD) is an important life limiting factor for aeroengine blades, with the leading edge of aerofoils particularly susceptible. Impacts due to small hard particle ingestion during takeoff and landing can reach velocities in the range of 60 to 500m/s and cause severe damage to aerofoils. Damage due to FOD is estimated at $4 billion annually for the aeroengine industry. The effects of FOD on high cycle fatigue (HCF) have been studied extensively for Ti-6Al-4V blade alloy mainly under constant amplitude loading, eg.[1-8], however little has been done under combined HCF and low cycle fatigue (LCF) until recently at Portsmouth [9,10]. The LCF loading, arises from the large cyclic variation of the conjoint centrifugal and thermal stresses, normally once per flight, while the HCF loading arises from small-amplitude vibrations. During flight these high-frequency cycles are usually superimposed on each major cycle, such that the fatigue integrity assessment must consider the effect of combined HCF and LCF loadings on crack growth [11].

2. MATERIAL AND EXPERIMENTAL PROCEDURE

Full details are given in [9].The material was plate titanium alloy Ti-6Al-4V, machined from blanks for the production of fan blades. Typical mechanical properties of Ti-6Al-4V plate at room temperature are: the Young's modulus 103 GPa, yield stress 860 MPa and tensile strength 980 MPa. FOD was simulated by firing a hardened steel cube (3.2 mm in edge length) onto the centre of a flat side surface of a plate specimen with a rectangular cross section of 6mm x 12mm. Figure 1 shows the geometry details of the specimen.

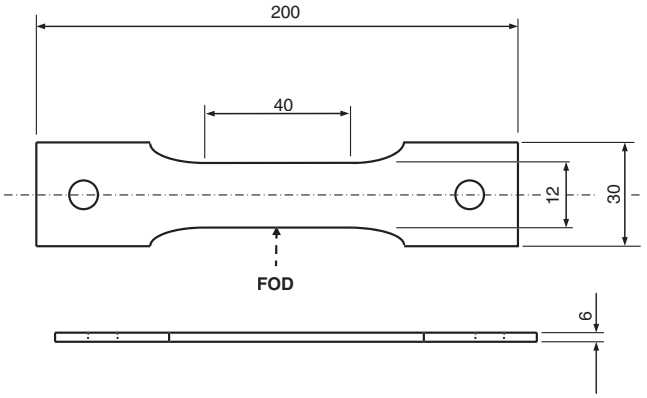

Fig. 1. Geometry of the plate specimen for FOD simulation.

The cube was impacted edge first onto one side of each specimen in the centre of the gauge length and its trajectory was at 90^0 to the impacted face. The notch takes a "V" shape in the specimen, representative of the "worst case" damage observed in aeroengine components.

FOD specimens were subsequently fatigued under tension-tension loading conditions using a hydraulic twin actuator 100kN fatigue testing machine. Figure 2 illustrates schematically the loading patterns used in the fatigue test programme.

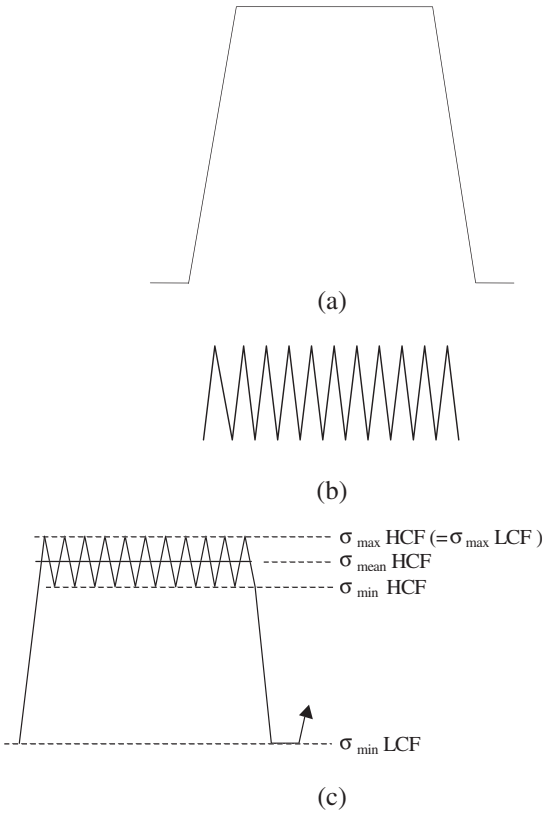

Fig. 2 Loading conditions

For LCF at a stress ratio of 0.01, the load cycle was a trapezoidal stress wave, where the rise and fall times were 1s while the times at maximum and minimum loads were 1.5s and 1.2s, respectively. For HCF with a stress ratio of 0.7, the load cycle was a sinusoidal stress wave with a frequency of 75 Hz. The conjoint action of LCF and HCF cycles, referred to as combined LCF+HCF loading, represents a simplified flight spectrum. In this simplified load sequence, a LCF cycle was superimposed by 1,000 HCF cycles, and the combined LCF and HCF was regarded as one loading block. To produce such a block the dwell time at maximum load of a LCF cycle was extended to 13.4 s to accommodate 1000 HCF cycles. In addition, the maximum stress ($\sigma_{max)}$ of HCF cycles was maintained the same as the maximum of the LCF cycles at 360 MPa.

Figure 3 shows da/dN for FOD – induced small cracks plotted against the stress intensity range ΔK for pure LCF or HCF loading. They are compared with growth rate data for long cracks obtained by fatigue tests on corner-cracked specimens as described earlier. For the HCF loading (R = 0.7), despite some scatter, most experimental points for the FOD specimens lay outside the long-crack data (CC), indicating a higher propagation rate of the FOD –induced small crack in comparison with the equivalent long crack. FOD-induced crack growth under the LCF loading (R=0.01) showed higher growth rate at low ΔK than that of CC, but tends to merge with long-crack results above a ΔK value of 10 MPa√m.

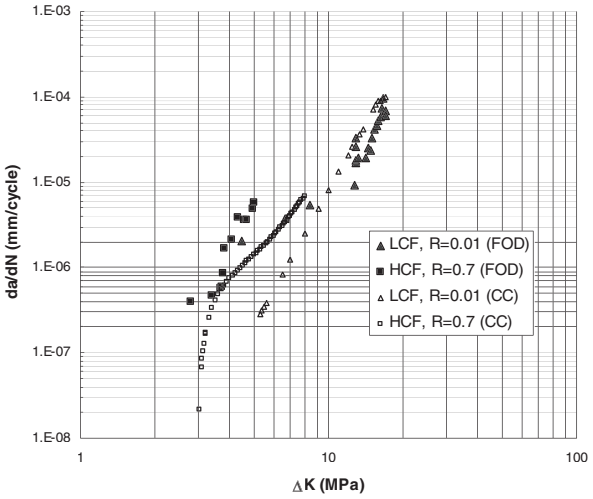

Fig 3. FCG rates of FOD and corner cracked (CC) specimens under the LCF and HCF loadings conditions.

Comparison of FCG rates between the FOD specimen and corner-cracked specimen under combined LCF + HCF loading is given in Figure 4. In the figure the growth increment per loading block, d*a*/d*B,* is plotted as a function of LCF stress intensity range (ΔK_{LCF}). Long-crack data (CC) shows that only LCF cycles contribute to the advance of the crack at the lower values of ΔK_{LCF}, since the FCG rate under combined loading equals that under LCF loading only. When ΔK_{LCF} exceeds an onset point (ΔK_{onset}), each minor cycle commences to contribute to the growth, which causes the growth rate to increase rapidly, deviating from the response to the application of a separate LCF loading. This result is consistent with those reported in previous studies [11]. The crack growth behaviour of the FOD specimen obviously deviates from the long-crack result. There exists

no apparent onset point ΔK_{onset}, since FCG rates under the combined loading are always much higher that those under the LCF loading only. This implies that HCF cycles can lead to crack extension even in the very early stage of fatigue life as well as LCF cycles.

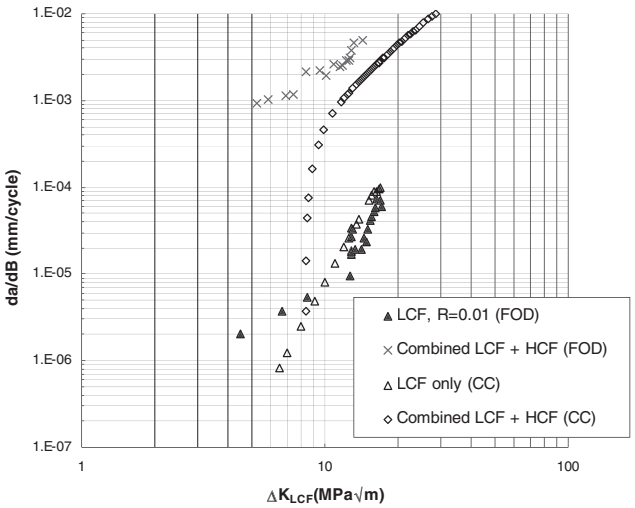

Fig. 4. FCG rates of FOD and corner cracked (CC) specimens under combined LCF/HCF loading conditions: R_{HCF} = 0.7, n =1000 : 1.

3. A TWO-PARAMETER CRACK GROWTH APPROACH

Fatigue crack growth equation

Recent work at Portsmouth [12] showed that the following equation can be used to rationalize both effects of stress ratio and temperature on threshold and FCG rates in forged Ti-6Al-4V:

$$\frac{da}{dN} = C(\Delta K)^n (K_{\max})^p G \tag{1}$$

where *C*, *n* and *p* are material constants. Similar to the NASGRO crack growth equation [13], the function $G = (1 - \Delta K_{thL} / \Delta K)^q$ is employed here to estimate near-threshold FCG rates in terms of ΔK_{thL}. ΔK_{thL} is a function of stress ratio *R*, and their relationship in Ti-6Al-4V at room temperature can be referred to [12]. Thus, Eq. 1 can be rewritten as

$$\frac{da}{dN} = C(\Delta K)^n (K_{\max})^p (1 - \Delta K_{thL} / \Delta K)^q \tag{2}$$

For rolled Ti-6Al-4V plate in this study, *C*, *m*, *n*, *p* are empirically obtained through best fits of the d*a*/d*N* – Δ*K* data for CC specimens (large cracks) described in [12]. By trial and error, *C* and *q* at room temperature are set to 2.83×10^{-9} and 0.25, respectively. The exponents *n* and *p* equal 2.8 and 0.65, respectively. The predicted FCG rate versus Δ*K* curves at *R* = 0.01, 0.7 and 0.9 are shown in Figure 5. The correlation between the predictions and experimental results is good for all the ratios.

To make Eq. 2 applicable to small cracks, ΔK and K_{max} should be replaced by ΔK_{mod} and $K_{mod,\,max}$. It gives

$$\frac{da}{dN} = C(\Delta K_{\text{mod}})^n (K_{\text{mod,max}})^p \times (1 - \Delta K_{\text{mod},th} / \Delta K_{\text{mod}})^q \tag{3}$$

As mentioned earlier $\Delta K_{mod,th}$ is constantly equal to ΔK_{thL} and crack is arrested if ΔK_{mod} is less than $\sigma\Delta K_{mod,th}$.

4. ANALYSIS FOR FOD –INDUCED SMALL CRACKS

Stress concentration and residual stresses from FOD

These are described in detail in [10]. Both stress concentration and residual stress from FOD can have an important influence on fatigue properties. A general and non-linear finite element code ABAQUS was used to model these factors. First ABAQUS/Explicit was employed for the time-dependent impact simulation. The possible contact interaction was defined via the contact pair approach in ABAQUS, which uses the master-slave algorithm to enforce the contact constraints, where the rigid surface is chosen as the master contact surface. The basic Coulomb friction model with isotropic friction is employed to invoke friction. The friction coefficient is assumed to be 0.1. The eight-node linear brick element with reduced integration was used for the plate specimen. Due to symmetry only half specimen was modelled.

The plate specimens are made from rolled Ti-6Al-4V plate. The Young's modulus and Possion's ratio of this material are 110 GPa and 0.34, respectively. Regarding plastic behaviours, Ti-6Al-4V has very low straining hardening, but is sensitive to the strain rate. The rate dependence of Ti-6Al-4V was expressed in a power-law form:

$$\dot{\varepsilon} = \dot{\varepsilon}_r \left(\frac{\sigma_Y(\dot{\varepsilon})}{\sigma_Y} - 1 \right)^n \tag{4}$$

where $\dot{\varepsilon}$ is the strain rate, $\sigma_Y(\dot{\varepsilon})$ is the strain-rate sensitive yield stress, and σ_Y is the yield stress at $\dot{\varepsilon} \sim 0$, and $\dot{\varepsilon}_r$ is a reference strain rate. $\dot{\varepsilon}_r$ is taken as $2\times10\text{-}4\ s^{-1}$ and *n* taken as 3.

It is important to note that only material deformation was modelled in the study, but material failure during the impact was completely ignored. It was because, as the authors found, such simulation, which allows elements to be removed from the mesh after a critical plastic strain is exceeded, always made the elements consistently fail and led to unrealistic results. As a result, the complex failure mechanisms seen in the formation of impact notches, such as tearing or shear bands, are not able to be adequately represented yet.

To characterize the final FOD geometry and the associated residual stresses needs a switch from the time-dependent explicit analysis used for impact simulation to the time-independent implicit analysis. The latter analysis, achieved

by using ABAQUS/Standard, removes both dynamic forces (inertia and damping) and boundary interaction forces and results in a residual stress state associated with static equilibrium. The FE predicted contour of the residual stress σr (or σ_x in the contour) was determined and is given in [13], which direction coincides with that of the subsequent fatigue loading, after a 200 m/s impact. It indicates that σ_r is compressive below the bottom of the impact site, and tensile immediately outside the damage rim. These tensile stresses can be very important to facilitate the growth of FOD-induced cracks as reported in [12], since superimposed on the fatigue load, it increases the maximum stress level. The model also predicts well on the slight plastic pile-up observed at the damage edges. The simulated maximum damage depth is about 0.58 mm, slightly short of the average measured value of 0.65 mm as reported in [12].

Utilizing the deformed three-dimensional mesh obtained after impact modeling (the residual stress were artificially removed), the local elastic stress concentration factor kσ ($k\sigma \equiv \sigma_x/\sigma_{app}$, where σ_{app} is the remote applied stress) associated with FOD can be determined, are along OD, and their k_t values. The result indicates that local stress level is approximately 45% higher than the applied stress at the impact edge (Point O). As the distance increase from the central line, σ_x tends to decrease and become to equal σ_{app} at the boundary of the specimen .

The residual stresses σ_r modeled [10], indicate an increase in σ_r as the location moves from the impact edge to the edge of the specimen. A previous study [14] reported that these initial residual stresses associated with FOD might not sustain because of their potential relaxation or redistribution during fatigue loading. The magnitude and rate of relaxation will be strongly dependent on the residual stress itself, applied loads and FOD-induced stress concentration. The stress relaxation is typically associated with the reordering of the dislocations and the occurrence with cyclic softening, i.e. the reduction in the flow stress during cyclic loading. In addition, upon the formation of a fatigue crack, the relaxation can further increase due to the stress-concentration effect and plasticity associated with the crack.

There is little information on stress relaxation in the present study, and it is just simply estimated that residual stress is 100% relaxed due to large $\Delta\sigma_{app}$ and the stress concentration effect for R=0.01, and there is no stress relaxation for R=0.7. It means that no residual stress effect is considered for R=0.01 for the analysis below. It was also concluded [10] that a major driving force in crack propagation immediately outside the impact edge is stress concentration since the residual stress lever is relatively low. As the crack grows away from this area, the effect of stress concentration diminished and the residual stress became a predominant driving force for propagation.

Fatigue crack growth calculation

According to above analyses, the maximum stress intensity factor and stress intensity factor range incorporating effects of small crack, stress concentration and residual stress can be respectively expressed as:

$$K_{\mathrm{mod}} = Fk_{\varepsilon}(\sigma_{app} + \sigma_r)\sqrt{\pi(a+a_0)/Q} \quad (5)$$

and

$$\Delta K_{\mathrm{mod}} = Fk_{\varepsilon}\Delta\sigma_{app}\sqrt{\pi(a+a_0)/Q} \quad (6)$$

The results of ΔK_{thL} and $\Delta\sigma_e$ of Ti-6Al-4V as a function of *R* have reported in [2,15], and therefore a_0 can be calculated and was found to equal 28.2 μm for the LCF loading with a stress ratio of 0.01 and 0.0542 μm for the HCF loading with a stress ratio of 0.7. Using Eqs. (5) and (6), the FCG rates are re-analysed in Figuress. 5 and 6 as a function of ΔK_{mod} and $(\Delta K_{\mathrm{mod}})^{n'}(K_{\mathrm{mod,max}})^{p'}(1-\Delta K_{\mathrm{mod},th}/\Delta K_{\mathrm{mod}})^{q}$ respectively, where $n'=n/(n+p)$ and $p'=n/(n+p)$. The values of *n*, *p q*, obtained from large crack results, are given above.

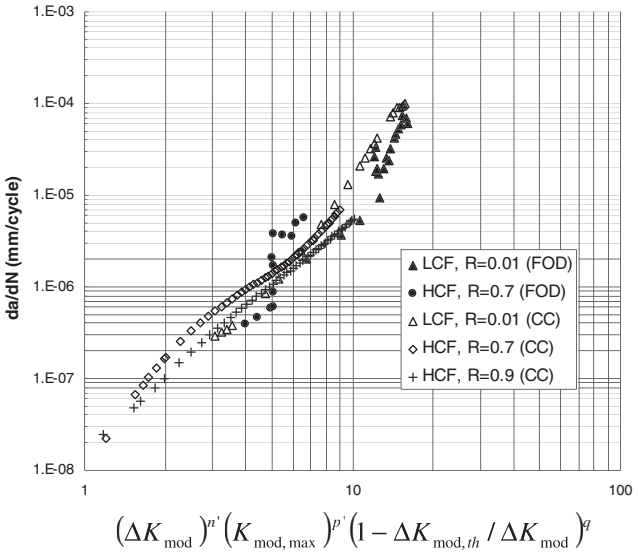

Fig. 5. Fatigue crack growth of large cracks and FOD-inducedsmall cracks under the LCF (R=0.01) or HCF (R=0.7) loading. The results are plotted against a two-parameter driving force $(\Delta K_{\mathrm{mod}})^{n'}(K_{\mathrm{mod,max}})^{p'}(1-\Delta K_{\mathrm{mod},th}/\Delta K_{\mathrm{mod}})^{q}$.

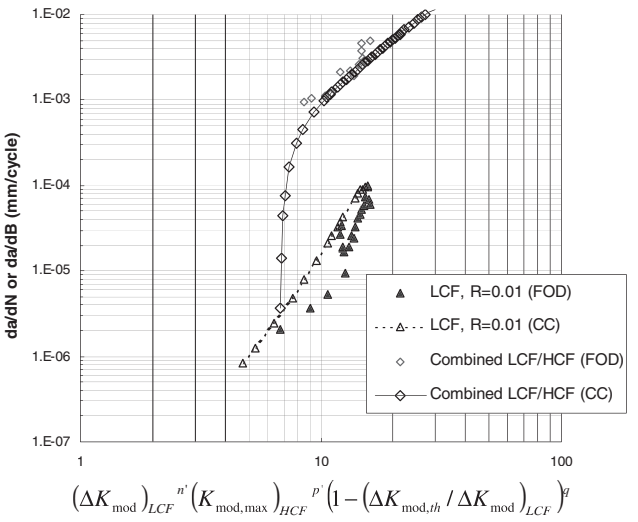

Fig. 6. Fatigue crack growth of large cracks and FOD-induced small cracks under a combined LCF/HCF loading (R_{HCF} = 0.7, n = 1000). The results are plotted against a two-parameter driving force $(\Delta K_{\mathrm{mod}})_{LCF}^{n'}(K_{\mathrm{mod,max}})_{HCF}^{p'}(1-(\Delta K_{\mathrm{mod},th}/\Delta K_{\mathrm{mod}})_{LCF})^{q}$.

Figure 6 shows that with the use of ΔK_{mod} incorporating the effects of small crack and stress concentration, all the values of corrected stress intensity ranges presented in this study become above $\Delta K_{mod,th}$, i.e. the large-crack fatigue threshold, ΔK_{thL}. At the LCF loading only (R= 0.01), FOD-induced crack growth data has merged into the large-crack curve within the experimental scatter. However, at the HCF loading (R=0.7) the overall FOD-induced small crack growth rates are still evidently higher than the corresponding large-crack results. This can be attributed to the influence of residual stress on $K_{mod,max}$, as described below.

5. CONCLUSIONS ON FATIGUE FROM FOREIGN OBJECT DAMAGE

FOD-induced small crack growth in rolled Ti-6Al-4V plate subjected to the combined LCF and HCF loadings has been predicted by a two-parameter crack growth equation together with a corrected stress intensity solution suggested by El Haddad et al. The following conclusions are drawn:

Fatigue threshold $\Delta K_{mod,th}$, defined according to El Haddad approach, is independent of crack length and the value of $\Delta K_{mod,th}$ constantly equals to ΔK_{thL} obtained from large-crack tests. Thus, $\Delta K_{mod,th}$ for any small crack can be easily obtained according to large-crack data.

FOD-induced small crack growth is fairly accurately predicted by a two-parameter crack growth equation together with a corrected stress intensity solution (the El Haddad approach). This method bridges the gap between large and small cracks and unifies them under a single crack growth law.

Rolled Ti-6Al-4V is sensitive to the load interaction under combined LCF/HCF loading conditions. This may attribute to the influence of LCF underloads to fatigue threshold and crack growth of HCF cycles. Two extra parameters representing the load interaction effect were thereby introduced into the crack growth equation, leading to a more reasonable and safe prediction for the onset of HCF contribution on crack advance.

PART B - SURFACE IMPROVEMENT
6. INTRODUCTION

It is well established that, in the absence of pre-existing cracks, 80 – 90% of total high cycle fatigue life is taken up by crack nucleation/initiation. Surface treatments such as shot peening impart a significant compressive residual stress into the surface of the material, this has the affect of lowering the peak and mean stress at the surface of the material and as a result will usually extend crack initiation life and therefore increase total fatigue life.

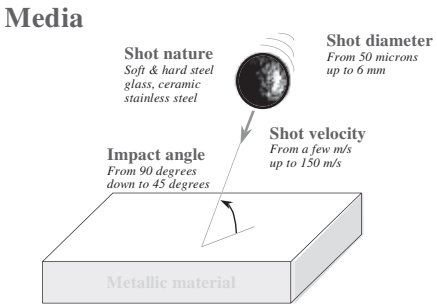

Fig. 7. Elements of shot peening process (Metal Improvement Co. Inc.)

Shot peening (Figure 7) is a cold working process, where the surface of the component is impacted, at high velocity, by small spherical particles called shot media. Each tiny piece of shot causes deformation to the surface. This deformation will strain harden the surface of the material. In order for this permanent indentation to be created, the surface of the material must plastically yield. Below this surface layer is a near surface elastic region which is trapped in a state of compression, therefore shot peening creates a surface that is not only cold worked, but contains a residual compressive stress in the near surface layer (Figure 8). Note also the tensile stress that is present below the compressive layer.

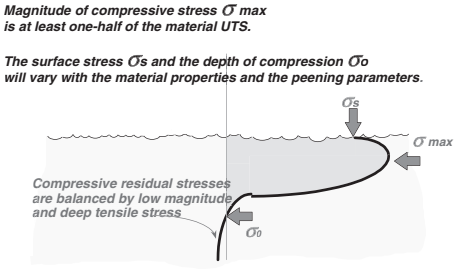

Fig. 8. Schematic residual stress profile of a peened surface. (Metal Improvement Co. Inc.)

Concern arises when the shot peened surface is damaged to some degree. Little information is known about the influence of damage on a shot peened surface and how it will affect the fatigue life of a component. With the exception of large internal defects it is expected that fatigue cracks initiate at the surface. Hence, it might be expected that fatigue crack initiation could be accelerated by damage

to shot peened surfaces and the beneficial effects of peening to fatigue life reduced.

7. SURFACE EFFECTS AND FATIGUE

It is well established that, in the absence of pre-existing cracks, 80 – 90% of total high cycle fatigue life is taken up by crack nucleation/initiation with the majority of cracks initiating at the surface [15]. Using shot peening to impart a significant compressive residual stress into the surface of the material will delay initiation and so extend fatigue life [16]. This advantage may be negated when the shot peened surface is damaged. Very little research has been conducted on the effects of damage to a shot peened surface, with much of the research focused on the use of shot peening over damaged surfaces [17].

High surface strength and good surface topography are important in resisting crack initiation. In general, fatigue life increases as the magnitude of surface roughness decreases, which minimises local stress raisers. High surface roughness will accelerate crack nucleation, leading to initiation [17]. However, more recently the effects of residual stresses are thought to be of more importance when modelling surface crack initiation life. It is thought that the majority of fatigue resistance, generated by shot peening, is due to compressive residual stresses with a small variable contribution from work hardening [eg.17].

Surface residual stresses, are induced by processes such as grinding, polishing, machining, and peening. Compressive residual stresses, generally, increase the fatigue life whilst tensile stresses decrease the fatigue life. Surface treatments such as shot peening, laser shock peening, burnishing, deep rolling, and various grinding methods improve fatigue performance by imparting a compressive residual stress [15-18].

8. SHOT PEENING

The process is usually adopted to delay crack initiation with little understanding of its affect on crack propagation and growth through residual stress profiles.

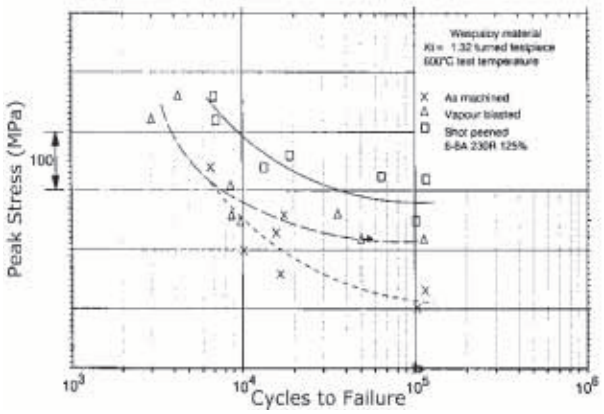

Fig. 9 Example of improvement in HCF life for the Waspaloy at 600C due to shot peening [16].

The process involves impacting the material surface with small hard particles at high velocity. Media hardness, velocity and coverage are the main variables in the shot peening process. The process of shot peening leads to the following important effects:

(a) Plastic deformation of the surface causes a peened effect, which depending on the variables used for the process, can lead to a detrimental increase in surface roughness which may result in early crack initiation.

(b) Strain hardening of the surface occurs leading to an increase in surface hardness and yield strength.

(c) A compressive surface residual stress profile is imparted into the plastically deformed surface layer, with a balancing internal residual tensile stress. This lowers the resultant maximum, minimum and mean stress levels leading to an increase in initiation life.

9. LASER SHOCK PEENING

The Laser Shock Peening (LSP) process [19] uses a high energy, pulsed laser to vaporise an opaque layer such as a black paint on the surface of the material. The ablation process generates a vapour, which is trapped between the sample and a transparent overlay of water, generating an extremely high localised pressure pulse for approximately 10 ns. This in turn causes a shock wave to propagate into the material. Since the amplitude of this pressure pulse is much greater than the dynamic yield stress of the material, the material is locally plastic deformed. To prevent the shock wave from exiting the back face of thin sections and causing material to spall off as the wave exits, the process is applied to both faces of a blade or specimen, with the two waves intersecting in the centre.

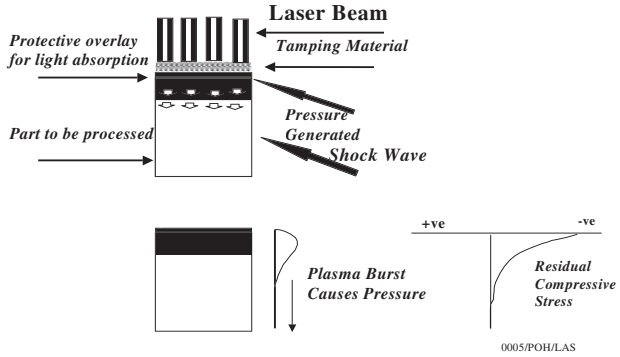

Fig. 10 Laser shock peening process. (Metal Improvement Co. Inc.)

The constrained plastic deformation that occurs under nominally uniaxial strain, produces deep compressive residual stresses normal to the impact direction at and below the surface . These stresses occur considerably deeper than can be obtained by conventional shot peening, as shown in (Figure 11).

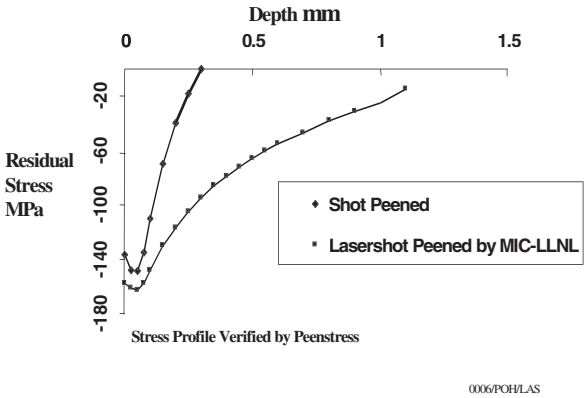

Fig. 11 Comparison of residual stress profiles for shot and laser shock peened Inconel 718 (Metal Improvement Co. Inc.)

10. DAMAGE AND PEENING

Very little research has been carried out on the effects of damage and shot peening. Nader [18] conducted tests with scratched 2024 Aluminium alloy and found fatigue life decreased and crack growth rates increased as the scratch depth was increased at all stress levels. This reinforces the need for further research into the area of damage to shot peened materials to try and gain a greater understanding of cracks initiating and growing through residual stress fields.

Many researchers state the importance of good surface topography and deep compressive residual stresses when designing for fatigue resistance, but very little work, has been done on the effects of damage to a shot peened surface caused by manufacturing installation, overhaul, or foreign object damage (FOD).

Rushchau *et al* [19] examined the effects of foreign object damage on shot peened and laser shock peened Ti-6AL-4V. A greatly extended propagation life was noted with the laser shock peened samples but multi-initiation of cracks was observed away from the site of foreign object damage, due to a poor surface condition induced by the laser shock peening process, although cracks did have a tendency to arrest.

(a)

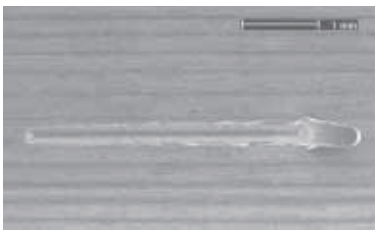

(b)

Fig. 12. (a) Kt 1.32 disc feature test-piece, (b) scratch damage within notch root.

11. RESEARCH ON FATIGUE /SHOT PEENING AT PORTSMOUTH

Material and Experimental Procedure

Fatigue tests were performed on a nickel base Superalloy provided by Rolls-Royce plc. The alloy was produced from an extruded and hot isostatically pressed powder material, which was forged, heat treated and machined to a disc containing a representative stress feature. The stress feature was designed to have an elastic stress concentration factor of K_t=1.32. Test-pieces containing the stress feature were wire-cut from the disc and finish machined (Figure 12(a)). These test-pieces therefore had a surface which was representative of an as-machined turbine disc

Test-pieces with as-machined and shot peened surface conditions were fatigue tested both with and without surface damage. Two shot peening conditions, which used different shot sizes and peening intensities were examined. The two sets of peening parameters were chosen to produce different depths of compressive residual stress and would typically be applied to different component features.
A 3mm long and 100μm deep scratch with a 90^o V groove at its root, was introduced on one surface of each test-piece (Figure 12(b)). This was machined at the root of the stress feature using an NC milling machine.

The fatigue tests were performed at stresses between 70% and 100% of the 0.2% proof stress of the material using load control at a temperature of 650^{o}C. These conditions are extreme and not typical for gas turbine disc operations. They were chosen as a compromise between representative operating conditions and laboratory expedience. A frequency of 0.25Hz, using a 1,1,1,1s, trapezoidal waveform, and constant load ratio R= 0.1 was used to simulate a basic flight cycle.

Crack initiation and propagation were monitored using the direct current potential difference (DCPD) technique. This method of monitoring crack initiation and growth involves passing a pulsed direct current through the test-piece whilst measuring the potential difference across the crack plane. As the crack propagates the potential difference increases due to increased resistance. Four fine platinum wires were attached to the specimen. One pair was attached either side of the scratch damage to monitor the increase in potential difference across the crack plane (V_{notch}). The other pair was attached to the face of the specimen away from the crack plane to act as a reference voltage (V_{ref}). The notch voltage was divided by the reference voltage to provide a normalized voltage ratio (Vr).

The relationship between voltage ratio (Vr) and crack depth was established for the test-piece geometry by changing the loading frequency during a fatigue test to produce changes in fracture surface appearance. This was achieved by applying a block of 0.25 Hz cycles, using the above test conditions, until initiation was complete. A block of dwell cycles, 0.01 Hz using a 97s dwell period at peak load, was then applied to generate a “beach mark” on the fracture surface. The dwell period gave rise to an increase in fatigue crack growth rate, effected by a change in crack growth

mechanism from predominantly transgranular to predominantly intergranular or mixed regime [20]. This change of mechanism created changes to the appearance of the fracture surface. By applying alternating blocks of the two frequency conditions a graduated fracture surface was generated and crack depths for given voltage ratios were measured (Figure 13).

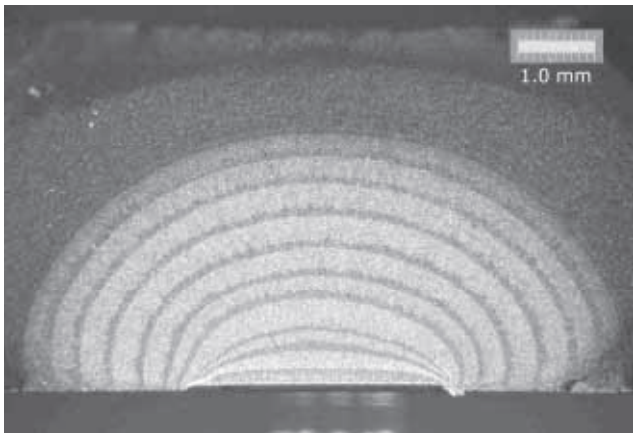

Fig. 13. Beach mark calibration from scratch damage (100μm) for a K_t=1.32 test-piece with surface in the as-machined condition.

Initiation was defined from the DCPD measurements by an arbitrarily defined deviation from the steady-state value of mean voltage ratio (Vr_{mean}), at which the value of Vr_{mean} exceeded 0.2% of the steady state value.

$$N_{initiation} = Vr_{mean} + ((0.2 \times Vr_{mean}) / 100) \quad (7)$$

12. RESULTS AND DISCUSSION

Residual stress measurements obtained by x-ray diffraction for both peening conditions are shown in Figure 14. A typical residual stress profile for the as-machined condition is also shown. The magnitude of the compressive residual stress is a function of the material and is equal for both peening conditions, however a much deeper compressive layer is imparted by the higher intensity peening condition.
A comparison of the peak stress ($stress_{nom} \times K_t$) data versus cycles to failure, for the as-machined and shot peened test-pieces, both with and without scratch damage, is shown in Figure 15. As expected there was a clear improvement in fatigue life for the shot peened tests compared to the as-machined tests. As expected there was also a fatigue debit when a scratch was introduced onto the as-machined test-pieces. However with the introduction of a scratch onto a shot peened surface there was a reduction in fatigue life, sufficient to negate the improvement in fatigue life from shot peening.

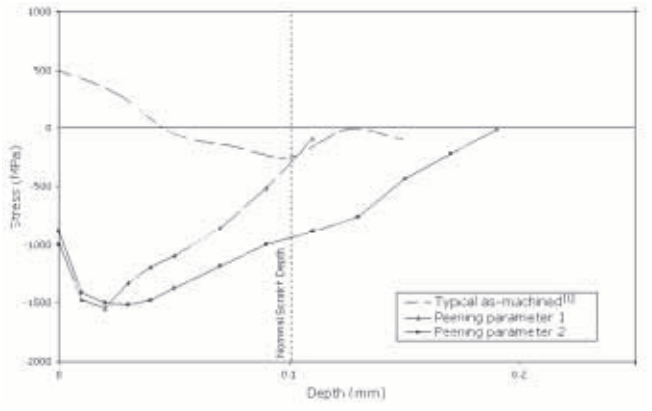

Fig. 14. Residual stress measurements of two peening parameters with different intensities and shot size, a representative as-machined profile is also shown.

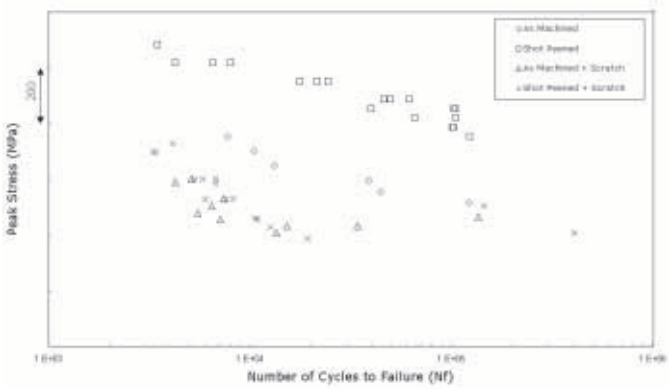

Fig. 15. Comparison of data for shot peened and as-machined test-pieces both with and without damage.

Surface measurements made on the calibration test-piece indicated that the initiation point of the DCPD technique corresponded to a crack of depth between 200 and 250μm, including the scratch depth. This crack extended along the entire length of the root of the scratch damage and grew from the linear scratch into a semi-circular shaped crack. The crack depth was defined as the deepest point of crack front from the surface of the test-piece.

From the appearance of the fracture surface, five distinct areas of crack development were observed. These areas in order of proximity to the scratch damage were as follows:

The first area exhibited multi-initiation of cracks along the scratch length and was characterised by ratchet markings close to the scratch root.

Area two involved the coalescence of micro-cracks into a crack, which extended along the length of the scratch. During this phase the crack was shallow with a maximum depth of about 100-150μm at the centre of the scratch root. At this point initiation was defined to be complete.

Within area three the crack growth was dominant at the mid-point of the crack length with relatively large increases in depth compared with surface growth. The fracture surface

changed from a shallow, semi-elliptical crack to a near semi-circular crack.

Area four exhibited an increase in crack growth rate at the surface so that the aspect ratio of the crack remained approximately constant.

Within area five, the crack growth showed increasing acceleration towards instability. This ended with the onset of fast fracture characterised by the presence of 45° shear planes.

The five areas of crack development outlined above were consistent with all tests containing a 100μm deep scratch. A graph of calibrated crack depth plotted against number of cycles is shown for a typical test in Figure 16. The crack depth measurement starts at 0.1mm, the depth of the scratch. There is no clear demarcation in the data between the different areas of crack growth, however, the approximate extent of the areas described above are shown.

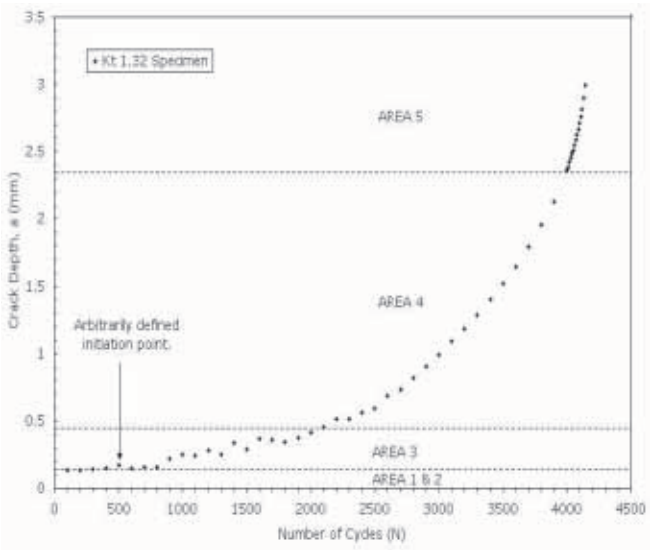

Fig. 16. Crack length, determined by DCPD calibration, versus cycles for a scratch damaged shot peened test-piece. The different phases of crack growth are indicated.

The introduction of a 100μm scratch led to earlier initiation compared to that of non scratched specimens for which the proportion of total life spent in the initiation phase was typically in the order of 70-90% of total life.

The graph in Figure 17 shows the proportion of total life spent in the initiation phase as determined by the 0.2% deviation from the DCPD Vr_{mean} value. This is shown for tests of increasing peak stress on scratch damaged test-pieces in the shot peened and as-machined condition. With increasing peak stress the *proportion* of a test spent in the initiation stage was seen to decrease for all tests irrespective of surface condition. This suggests that the shot peening used had no influence on initiation life for the tests with 100μm surface damage.

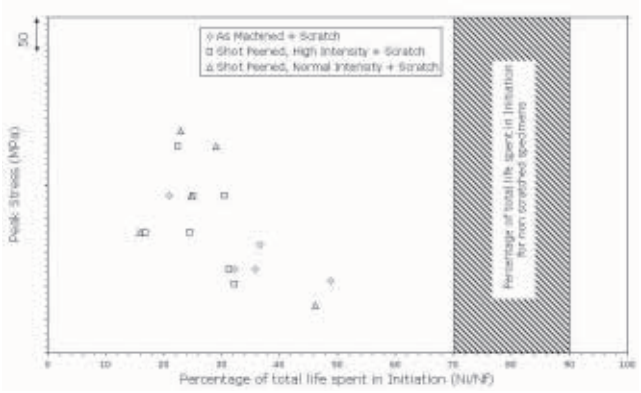

Fig. 17. Percentage Initiation lives for test-pieces with different surface conditions at 650°C with scratch damage in the order of 100μm depth.

Measurements of the compressive residual stress imparted by both shot peening parameters are show in Figure 14. The 100μm deep scratch lies within the compressive layer for either of the shot-peening parameters. The scratch however is deeper than the position of the peak compressive stress for each peening parameter (40-50μm). It is suggested that under the test conditions used, it is only required for the damage to be deeper than the peak compressive stress for the benefits of shot-peening to be negated. In negating the effects of shot peening some further effects of the scratch should be considered. Firstly the action of cutting the scratch will itself impart a residual stress profile, possibly similar to that of the as-machined profile shown in Figure 14. Secondly, at the tip of the scratch there is an elastic stress-concentration whose magnitude increases with scratch depth and applied load. This will contribute to decreasing the fatigue benefits derived from the shot peening. Finally, it is thought that some stress relaxation of the compressive layer will occur at a testing temperature of 650°C. A marked reduction in compressive residual stress depth due to relaxation could lead to a 100μm deep scratch being completely beyond the benefits of the compressive layer.

13. CONCLUSIONS ON SURFACE IMPROVEMENT BY SHOT PEENING

For the tests presented here, the conditions of stress and temperature would be considered extreme for current gas turbine applications. However, a significant improvement in total cyclic life of an order of magnitude was achieved under these conditions by shot peening. This improvement was almost entirely negated by the 100μm surface scratch applied. This was despite the fact that the scratch depth did not extend beyond the nominal compressive layer generated by the shot peening.

Accurate definition of the residual stress fields generated by scratch damage is required to fully explore the relationship between both shot peening and scratch damage. An investigation into stress relaxation due to temperature is also required.

ACKNOWLEDGEMENTS

The authors would like to thank EPSRC, MOD and Rolls-Royce plc for funding and ongoing support.

REFERENCES

[1] Ritchie, R.O., Boyce, B.L., Campbell, J.P., Roder, O., Thompson, A.W., Milligan, W.W., *Int. J. Fatigue*, **21** (1999), 653.

[2] Hamrick, J.L., Nicholas, T., Proc 4th National Turbine Engine HCF Conference, 9 –11 February, (1999), Monterey, California.

[3] Mall, S., Hamrick, J.L., Nicholas, T., *Mechanics of Mat.*, **33** (2002) 679.

[4] Peters, J.O., Ritchie, R.O., *Mat. Sci. and Eng.,* A319-321 (2001) 597.

[5] Peters, J.O., Ritchie, R.O., *Int. J. Fatigue* **23** (2001) 413.

[6] Peters, J.O., Boyce, B.L., Chen, X., MaNaney, J.M., Hutchinson, J.W., Ritchie, R.O., *Eng. Fracture Mechanics 69* (2002) 1425.

[7] Thompson, S.R., Ruschau, J.J., Nicholas, T., *Int. J. Fatigue* **23** (2001) 405.

[8] Martinez, C.M., Eylon, D., Nicholas, T., Thompson, S.R., Ruschau, J.J., Birkbeck, J., Porter, W.J., *Mat. Sci. and Eng.* **A325** (2002) 465.

[9] Ding, J., Hall, R.F., Byrne, J. and Tong, J., *Int. J. Fatigue.* **29** (2007) 1339.

[10] Ding, J., Hall, R.F., Byrne, J. and Tong, J., *Int. J. Fatigue*. **29** (2007) 1339.

[11] Powell, B.E., Duggan, T.V. and Jeal, R.H., *Int. J. Fatigue*, **4** (1982) 4.

[12] J Ding, R Hall and J Byrne, *Int. J. of Fatigue*, 27 (2005) 1551.

[13] *NASGRO 3 Reference Manual*, NASA, Johnson Space Centre Document JSC-22267B, Version 3.0.20 May 2002.

[14] Boyce BL, Chen X, Peters JO, Hutchinson JW, Ritchie RO., *Mat. Sci. and Eng.* **A349** (2003) 48.

[15] Eftekhari, A., Talia, J. and Mazumdar, P., *Mater Sci and Eng* A199 (1995) L3.

[16] Webster, P.S. and Cunningham, T.P., Shot Peening: Techniques and Applications, Eng. Mat. Advisory Services Ltd "The application of shot peening technology in the aero engine industry" (1993) ed. Marsh, K.J., London.

[17] Talia, M., Talia, J.E., High Cycle Fatigue of Structural Materials, (1997) 409.

[18] Nader, N., 'The effect of Scratches on the Fatigue Life and Fatigue Crack Growth of Al 2024-T3 clad', PhD thesis, (1993) The Witchita University.

[19] Ruschau, J., John, R., Thompson, S.R. and Nicholas, T., *Int. J. of Fatigue* **21** (1999) :S199.

[20] Dalby, S., Tong, J., Byrne, J., Effects of loading waveform on fatigue crack growth at elevated temperature, *Proceedings of the 1st International Conference on Component Optimisation,* (1999) Edited by W.J. Evans, R.W. Evans, M.R. Bache, EMAS, West Midlands, England.